Large mode area double-clad ytterbium-doped spun tapered fiber

Andrei Fedotov,[1,*] Vasilii Ustimchik,[2] Joona Rissanen,[2] Teppo Noronen,[2] Regina Gumenyuk,[1] Alexander Kolosovskii,[3] Victor Voloshin,[3] Igor Vorob'ev,[3] Yuri Chamorovskii,[3] and Valery Filippov[2]

[1]Tampere University, Kalevantie, 33100 Tampere, Finland
[2]Ampliconyx Ltd, Lautakatonkatu 18, 33580 Tampere, Finland
[3]Kotel'nikov Institute of Radio Engineering and Electronics (Fryazino Branch) Russian Academy of Sciences, Vvedenskogo Sq. 1, 141190 Fryazino, Russian Federation
*Corresponding author: andrei.fedotov@tuni.fi

We performed a comparative study of Yb-doped double-clad large mode area (MFD = 31 μm) spun tapered fibers with different pitch lengths. A novel type of spun tapered fibers with constant pitch lengths of 7.5, 15, and 30 mm, internal birefringence as low as $\sim 10^{-8}$, and perfect output beam quality ($M^2 < 1.2$) has been manufactured and investigated. We demonstrated the efficient direct amplification of a picosecond pulsed signal (95 ps/100 MHz, 1064 nm) in the spun active tapered fiber with optimized geometry providing an average output power of 71 W (gain 32 dB, 74% slope efficiency). Efficient green light generation (λ = 532 nm) with 17 W average power (1.7 μJ) and 80 pm linewidth was demonstrated using the developed master oscillator power amplifier system.

1. INTRODUCTION

The technology of high-power pulsed fiber amplifiers requires large mode area (LMA) polarization-maintaining (PM) active fibers. Currently, three main types of fibers are used for these purposes: LMA PM fibers with a low numerical aperture (NA) [1], microstructured active fibers [2], and tapered double-clad fibers (T-DCF) [3]. Polarization maintaining in all types of these fibers is achieved by inducing strong internal stresses (PANDA or stressed cladding technology). The high-temperature sensitivity of birefringence in active fibers with strong internal stresses is a significant disadvantage of all these types of fibers [4–7]. It is especially important for active fibers because they are always subject to inevitable internal heating mainly caused by a quantum defect [8]. As a rule, the strong pumping of active PM fiber leads to a rather rapid deterioration of the polarization extinction ratio (PER) [9].

The temperature sensitivity of the state of polarization (SOP) is defined by the value of the induced internal birefringence itself [4–7]. To solve the problem of SOP drift caused by the internal heating of PM active cladding-pumped fiber, we recently proposed active fibers with low intrinsic birefringence (so-called active spun T-DCF or sT-DCF) [10–13]. In [10–13], an Yb-doped sT-DCF with a 26 μm mode field diameter (MFD) and 35 μm core diameter was demonstrated. The sT-DCF demonstrated in [10–13] had spinning pitch varied along the length within the 6 to 13 mm range.

For this paper, we have fabricated an active sT-DCF with an MFD of 31 μm (44 μm core diameter) and different pitch lengths (7.5, 15, and 30 mm) constant along the entire length of active tapered fiber. We analyzed how the pitch length of sT-DCF affects parameters of the output radiation: degree of polarization (DOP), amplification efficiency, and output mode content (beam quality). The 95 ps/100 MHz master oscillator power amplifier (MOPA) based on sT-DCF with an average output power of 71 W and stable output SOP is demonstrated. Second-harmonic generation for output radiation from the active sT-DCF as a gain media is presented and studied.

2. EXPERIMENT

A. Manufacturing of Spun T-DCF with a Constant Pitch Length

To produce sT-DCF, the Yb-doped preform with a 1:11 core-to-cladding diameter ratio and step-index core (NA ~ 0.1) was assembled. The in-core absorption was measured as much as 550 dB/m at 976 nm. To improve clad pump absorption in sT-DCF, the first cladding was four times truncated into a square shape with rounded corners, as shown in Fig. 1(a).

sT-DCF was manufactured by using a similar technology previously exploited for passive [14] and active spun tapered fibers [10–13]. During the drawing process, the preform was fed into a high-temperature furnace with a certain speed varied

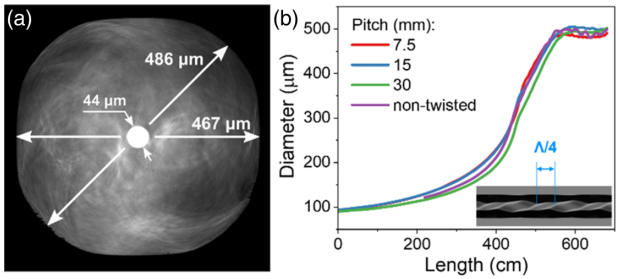

Fig. 1. (a) End face view of the wide side of sT-DCF. (b) Outer cladding diameter of sT-DCF versus length.

in time to form the required tapered longitudinal profile. The only difference from [10–13] is that now the angular velocity of preform rotation also varied in time in accordance with fiber drawing speed. The key element of the drawing tower for the production of the sT-DCF was the high-precision spinning mechanism with a wide range of rotation speed and precise alignment of a preform to avoid preform eccentricity relative to the drawing axis. All above-mentioned parameters (i.e., speed of preform feed, angular velocity of preform rotation, and speed of drawing) were changed in accordance with a predetermined algorithm to obtain a given constant rotation pitch along the length of the sT-DCF.

Thus, the cladding diameter varied from 486 μm down to 90 μm (tapering rate T = 5.4) along the length of 6.7 m. The longitudinal profiles of each sT-DCF are shown in Fig. 1(b). We have manufactured three different types of sT-DCF with the same lengths and similar longitudinal profiles but with different pitch lengths: 7.5, 15, and 30 mm [Fig. 1(b)]. Also, for comparison purposes, the standard tapered double-clad fiber (T-DCF) without any rotation has been drawn as well. All fibers (sT-DCFs and T-DCF) were coated by low-index primary reflecting coating (NA ~ 0.4) and secondary protecting acrylate coating.

Pump radiation at 976 nm has been launched into the wide end of tapered fiber by a lens with NA = 0.15. The overall pump power losses due to Yb absorption and vignetting for all sT-DCFs and standard T-DCF have been measured and are shown in Table 1.

Table 1. Pump Losses for Different Tapered Fibers

Pitch Length, mm	Pump Power Losses, dB/m
7.5	3.46
15	2.51
30	2.00
Standard	1.70

B. Beam Properties: Spatial Distribution and M^2

For all experimental samples of sT-DCFs, the MFD, beam quality, and spatial polarization beam uniformity have been measured. Figure 2 shows the results of the near-field distribution and M^2 measurements for the sT-DCF with different pitch values and similar standard T-DCF drawn without preform rotation. The main parameters of the measured beams are listed in Table 2.

The spatial uniformity of SOP and PER of the output beam in the amplification regime (40 W of pump power) were studied in the following experiment. A Glan–Taylor polarizer was installed in front of the beam profiler, and a series of images at a different azimuth of polarizer was taken. Figure 3 shows the intensity distribution of the output beam after passing through the polarizer for six different orientations of the polarizer (0, 15, 30, 45, 60, and 90°). Fibers were coiled with a diameter of 30 cm. No cooling measures were taken.

In cases of standard T-DCF and sT-DCF with 15 and 30 mm pitch, the intensity of fundamental mode decreased uniformly with rotation of the polarizer. This indicated that the beams were single-mode and that polarization was uniform across the core. In contrast, output radiation of sT-DCF with 7.5 mm pitch consists of high-order modes. Even when the polarizer blocked the fundamental mode, the higher-order modes remained visible. This means that the SOP of HOMs differs from the linearly polarized fundamental mode.

Far- and near-field patterns for a multimode pump were investigated and are depicted in Fig. 4. It was observed that localization of the pump radiation; therefore, pump absorption is directly dependent on the pitch value. Preform rotation during fiber drawing leads to the appearance of internal torsional mechanical stresses across the sT-DCF cross-section structure, which, in turn, cause spatial modulation of the refractive index due to the elastic-optical effect.

This leads to the formation of additional parasitical waveguides in the sT-DCF cladding and results in the delocalization of pump radiation [13]. The distribution of the pump radiation intensity in the near and far field at the output of fibers with different degrees of twisted (nontwisted and with 7.5, 15, and 30 mm pitch) is shown in Fig. 4.

D. Picosecond MOPA System with sT-DCF

To compare the amplification properties of three spun tapered double-clad fibers, we built a MOPA system, as shown in Fig. 5. A commercially available 95 ps gain-switched laser diode was used as a seed laser. The repetition rate was set to 100 MHz. A linearly polarized signal with the linewidth of 100 pm was

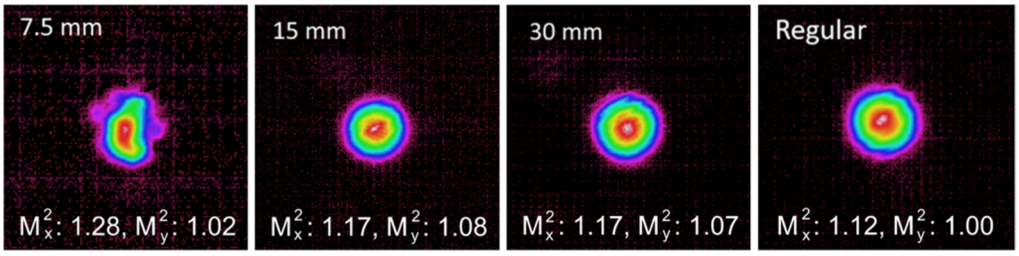

Fig. 2. Near-field pattern and M^2 for sT-DCF with different pitches and standard T-DCF.

Table 2. Beam Properties for sT-DCF with Different Pitches (7.5, 15, and 30 mm) and Standard T-DCF

Pitch Length, mm	Core Diameter, μm	Beam Shape	Spatial Polarization Distribution	MFD, μm	M_x^2 / M_y^2
7.5	44	Asymmetrical (few modes)	Impure uniform	30 × 22	1.28/1.02
15	44	Round	Uniform	30	1.17/1.08
30	44	Round	Uniform	31	1.17/1.07
Standard	44	Round	Uniform	31	1.12/1.00

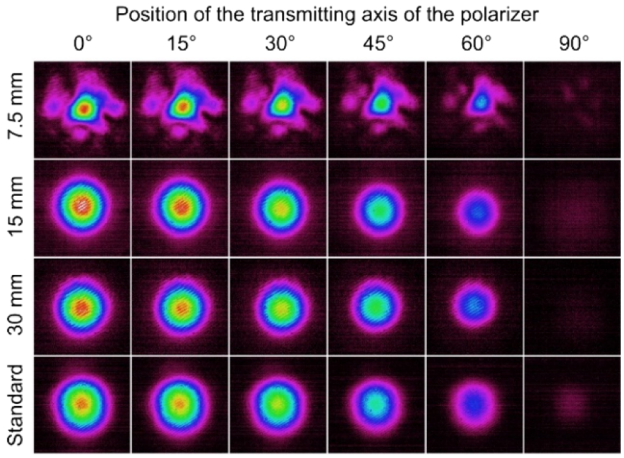

Fig. 3. Spatial polarization uniformity in the near field of the output beam for sT-DCF with different pitches (7.5, 15, and 30 mm) and standard T-DCF.

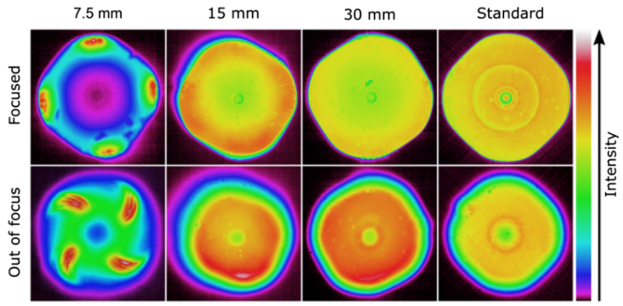

Fig. 4. Pump radiation intensity distribution in a cross-section of sT-DCFs with different pitches (7.5, 15, and 30 mm) and standard T-DCF.

preamplified up to average power of 40 mW and launched to the narrow end of the sT-DCF through the high-power isolator. sT-DCF was pumped by a 976 nm laser diode only from the wide end using a free space assembly consisting of the dichroic mirror to separate the pump and signal wavelengths and two aspherical lenses. We only cooled the first 15 cm from the wide end of the tapered fiber to prevent damage of the polymer coating due to intense pumping. The rest of the tapered fiber was coiled on a metal plate and not actively cooled. We deliberately tested the spun tapered fibers under harsh conditions in order to reveal the temperature dependence of the polarization state.

To measure and visualize the temperature distribution in the sT-DCF when pumped from the wide side, we used a thermal imaging camera. Figure 6(a) shows part of the setup, including the cooling holder, lens, and part of the wide side of sT-DCF. The image was taken at the maximum pump power of 100 W. Temperature of the cooling holder was kept at 18°C in contrast with the plate temperature. The holder had a square groove, which provided more efficient cooling compared with the plate, where thermal contact with the fiber was minimal. The temperature of sT-DCF at different points was measured as a function of pump power [Fig. 6(b)]. The hottest point had a temperature of 40°C. The maximum temperature gradient (over the first 2 cm of sT-DCF) reached 20°C [Fig. 6(c)].

The highest output power of 71 W was obtained using sT-DCF with 30 mm pitch, while the lowest output power of 34 W was reached in the case of sT-DCF with 7.5 mm pitch [Fig. 7(a)]. As can be seen from Fig. 7(b), slope efficiency increases with pitch length increasing. At the same time, one can assume that shorter pitch provides better cladding mode mixing and therefore improves absorption [Fig. 7(b)]. However, it was observed experimentally that pump localization got worse in sT-DCF with decreasing pitch (described above). Moreover, the slope efficiency of the sT-DCF decreases with decreasing pitch [Fig. 7(b)]. Therefore, it may be concluded that pump leakage

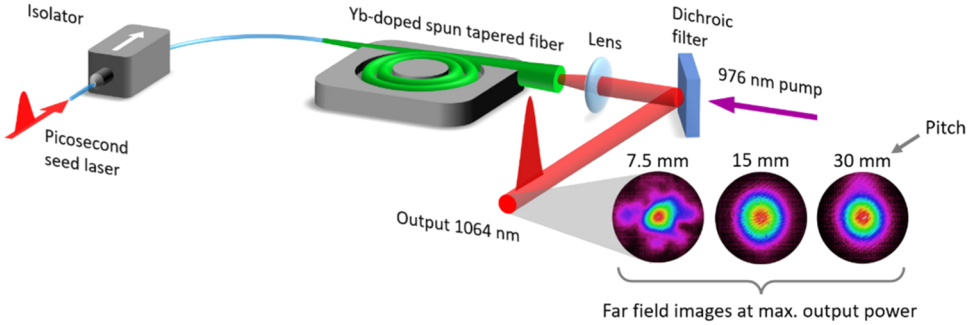

Fig. 5. Scheme of the experimental setup and images of the output beam at maximum output power for sT-DCF with 7.5, 15, and 30 mm pitch.

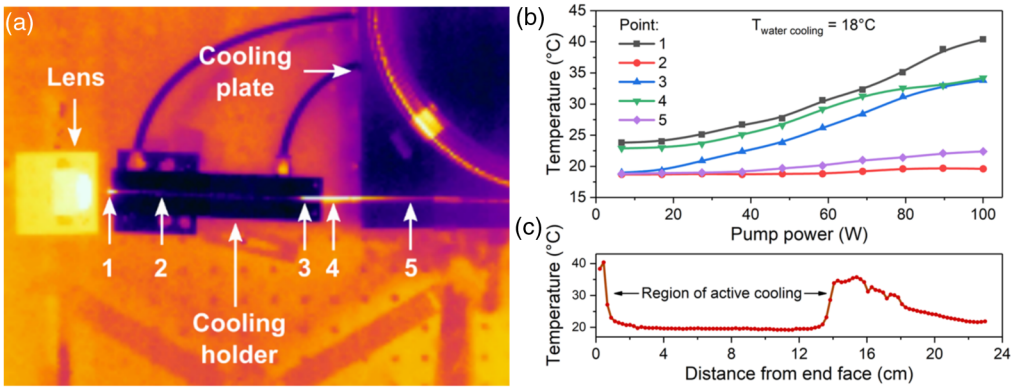

Fig. 6. (a) Thermal image of the wide end of sT-DCF with 30 mm pitch. (b) Temperature change at five points of the fiber during pumping. The numbering corresponds to the number in (a), which indicates the points of temperature measurement. (c) Temperature distribution over the first 23 cm of the wide end of the sT-DCF at the maximum pump power of 100 W.

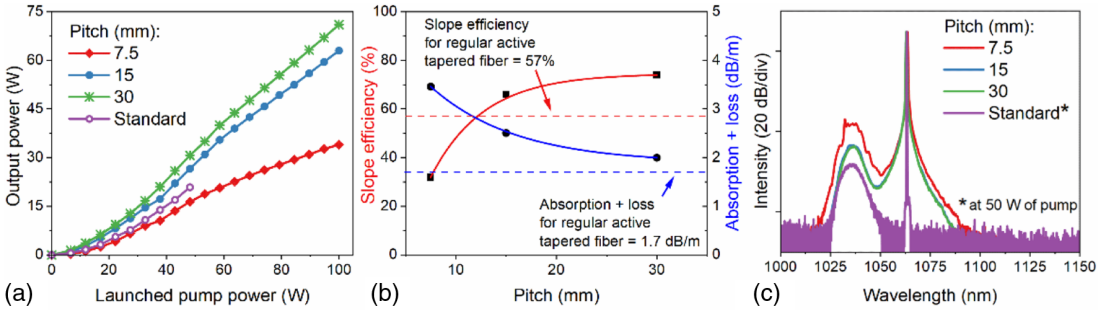

Fig. 7. (a) Output power versus pump power. (b) Efficiency as a function of the pitch of sT-DCF. (c) Spectrum of the output amplified signal for 7.5, 15, and 30 mm sT-DCF and standard T-DCF.

(vignetting) grows faster with decreasing pitch of sT-DCF than a significant cladding mode mixing occurs. On the other hand, higher slope efficiency was observed in the MOPA system based on sT-DCF in contrast with standard nontwisted T-DCF (formally with infinite pitch). At the same time, slope efficiency should be a continuous function by its nature for all values of the pitches. Hence, overall efficiency should reach at least one maximum with a pitch value in the middle range, i.e., about 30 mm in our case [Figs. 7(a) and 7(b)]. Figure 7(b) shows attenuation of pump power as a combination of absorption and loss during propagation from the wide to narrow end in tapered fiber samples. Stronger ASE for 7.5 mm sT-DCF [Fig. 7(c)] also indicates that the signal in the core experienced higher losses compared with 15 and 30 mm pitch. sT-DCF with 30 mm pitch delivered the highest output power of 71 W and spectrum with ~30 dB ASE-to-signal contrast. The slope efficiency and gain of this sT-DCF-based MOPA were 74% and 32 dB, respectively. Standard T-DCF was pumped only up to 50 W because of too-low absorption. This led to overheating of the cladding mode stripper; thus, we were forced to limit pump power.

Over the entire output power range, we have measured the SOP for the output signal of MOPA based on sT-DCF samples with three different pitches and standard T-DCF. A set of measurements was made when a linearly polarized signal was launched into tapered fiber through a narrow side using free-space coupling (Fig. 8). Among all sT-DCF, the lowest output signal DOP (without pumping) of 92.6% was demonstrated by sT-DCF with 7.5 mm pitch. At maximum output power, it decreased to 84%. This was caused by the excitation of higher-order modes that had different SOP (Fig. 3). Another factor is higher ASE than in other tapered fibers.

In the case of sT-DCF with 15 and 30 mm pitches, DOP decreased from 98% to 90% and from 96% to 82.6%, respectively, in the pump power range 0–100 W. The smallest fluctuation of azimuth and ellipticity was observed at the output of 30 mm sT-DCF: 3.9% and 0.9%, respectively (Table 3). Because standard T-DCF was pumped only up to 50 W, for comparison purposes, Table 3 is split into two parts. Absolute changes in DOP and SOP are shown in two pump power ranges of 0–50 and 0–100 W. Standard nontwisted T-DCF demonstrated the biggest absolute changes in azimuth and ellipticity in the pump power range 0–50 W.

3. DISCUSSION

Doping a fiber core by rare-earth ions and the process of fiber drawing itself is accompanied by the formation of strong local mechanical stresses in the core, which are inhomogeneous both in cross-section [15–18] and along the fiber length [19,20]. Reference [15] demonstrated that doping by Yb^{3+} ions leads to significant mechanical stresses and local changes in the refractive index up to 10^{-4}. Thus, the polarization properties of an active optical fiber are substantially transversely and longitudinally inhomogeneous. Light depolarization, caused

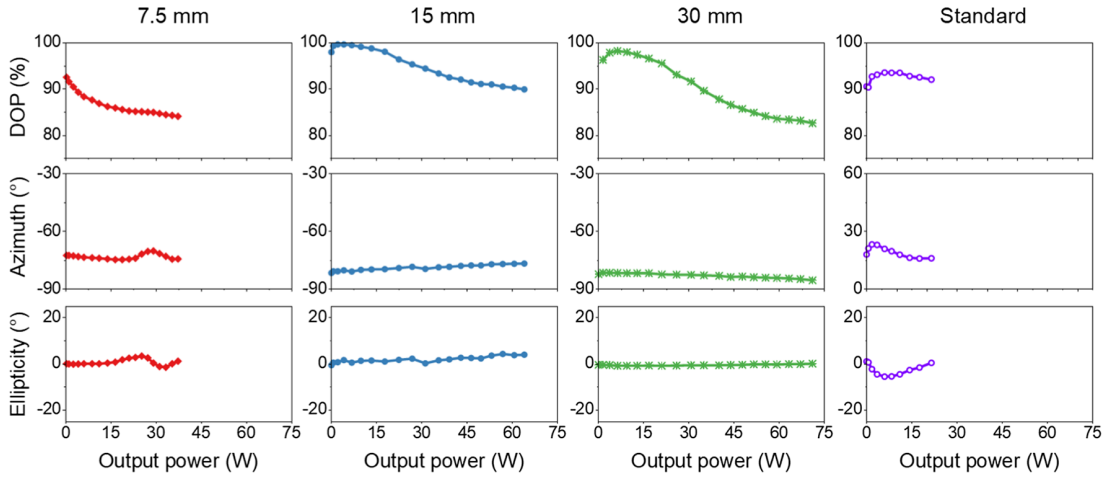

Fig. 8. Evolution of linear polarization state at the output of sT-DCF depending on the output power for 7.5, 15, and 30 mm sT-DCF and standard T-DCF. Degree of polarization, azimuth, and ellipticity of output radiation as a function of output power.

Table 3. Absolute Changes in DOP, Azimuth, and Ellipticity for 7.5, 15, and 30 mm sT-DCF and Standard T-DCF in Two Pump Power Ranges of 0–50 W and 0–100 W

	0–50 W Pump				0–100 W Pump			
Pitch, mm	**7.5**	**15**	**30**	**Nontwisted**	**7.5**	**15**	**30**	**Nontwisted**
Δ DOP, %	6.7	4.3	6.6	3.2	8.5	9.8	15.6	–
Δ Azimuth, °	2.2	3.2	1.0	7.3	4.8	4.8	3.9	–
Δ Ellipticity, °	1.0	2.9	0.4	6.5	5.2	5.9	0.9	–

by the doping-induced internal stresses, is the main obstacle for the development of an active fiber suitable for the efficient amplification of polarized light [12].

The goal of this work is to create an LMA active tapered fiber delivering stable SOP with good amplification properties. For this, we used the spun fiber approach, earlier proposed for passive fibers [21,22]. In an active fiber twisted hundreds of times, a polarized light on average spends the same time in the "fast" and "slow" axis of each local birefringence; as a result, spun fiber becomes close to a uniform perfect fiber without any birefringence (or very small birefringence) with polarization modes near degenerated by a propagation constant [12,21,22]. As follows from our experimental results, the output of the amplifier with sT-DCF has a DOP close to 100%, and SOP is almost insensitive to the internal heating process caused by a quantum defect (Fig. 8).

sT-DCFs with the same length (6.7 m) but different pitch lengths (7.5, 15, and 30 mm) constant along the length were manufactured from the same preform in the frame of current work. At the same time, for comparison, a standard T-DCF with the same longitudinal profile was drawn from the same preform without any spinning. In our experiments, we compared sT-DCF with different pitches via the following parameters:

- Output beam shape, M^2, and mode content.
- Polarization properties of sT-DCF output radiation: SOP, DOP. Type of polarization eigenstates. Stability of output SOP.
- Internal birefringence values (Table S1 in Supplement 1).
- Double-clad pump absorption and features of pump power vignetting in sT-DCF with different pitches.
- Efficiency in picosecond MOPA at 1064 nm.

At first glance, we can expect better polarization performance (better DOP and lower internally induced birefringence) for sT-DCF with shorter pitch length: more revolutions for the same length give better averaging. Another argument in favor of a shorter pitch is that twisting a double-clad fiber is known to significantly improve pump cladding absorption [23]. Results of measuring the output beam quality for sT-DCFs with different pitches are shown in Fig. 2 and in Table 2. Experimental results indicate that the output beams of sT-DCFs with 15 and 30 mm pitch and nontwisted (standard) are nearly Gaussian single-mode ($M^2 = 1.17/1.08$) with SOP homogeneous in the cross-section. The standard T-DCF output beam also has excellent spatial properties ($M^2 = 1.12/1.00$). At the same time, the output beam of sT-DCF with 7.5 mm pitch is spatially (and polarization) inhomogeneous (few transverse mode beam), with $M^2 = 1.28/1.02$. The reason for this can be explained as follows.

The cladding of an active double-clad fiber is usually shaped to improve pump absorption [24]. Rotation of four times truncated (in our case) preform during fiber drawing leads to periodic longitudinal modulation of the cladding diameter with a period of Λ/m (Λ is the pitch length [see Fig. 1, inset]; $m = 4$ is the number of clad truncations). As a result, sT-DCFs with 7.5, 15, and 30 mm pitches have longitudinal modulation periods of 1.88, 3.75, and 7.5 mm, respectively. Thus, mode coupling occurs and results in the transfer of fundamental mode power to higher-order modes [25]. The output radiation becomes multimode, which is highly undesirable.

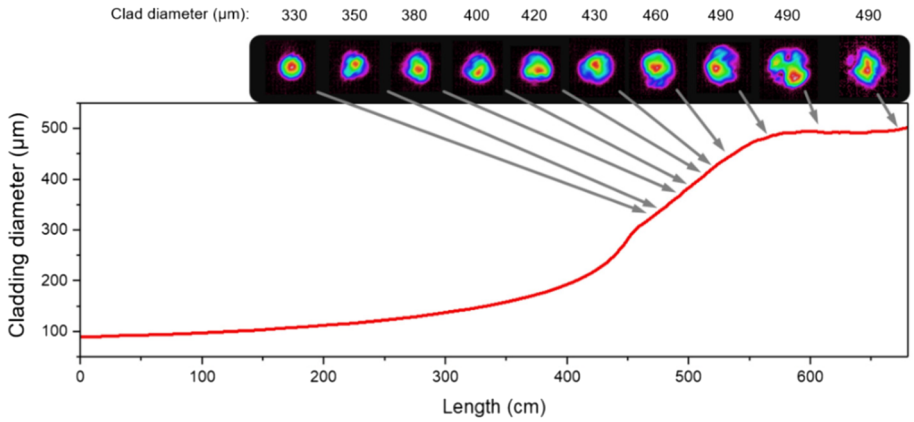

Fig. 9. Near-field pattern in the different cross-sections of sT-DCF with 7.5 mm pitch.

The multimode output beam of sT-DCF with a 7.5 mm pitch is depicted in Fig. 2. In order to find the point where the mode content is changed, we consistently shortened the 7.5 mm pitch sT-DCF until the output beam became Gaussian-shaped. This point corresponds to the 33 μm core diameter (cladding 330 μm, MFD 22.5 μm, fiber length 4.8 m). Mode field distributions in the near field for each cross-section are shown in Fig. 9.

For periodical perturbation, mode coupling becomes resonantly effective in the event the propagation constants' difference of coupled modes is equal to the spatial modulation frequency of fiber's clad diameter [25]:

$$\beta_i - \beta_j \sim 1/L_{\text{mod}}\,, \qquad \textbf{(1)}$$

where $L_{\text{mod}} = \Lambda/m$ is the period of the longitudinal modulation of a clad diameter ($m = 4$ for square-shaped clad). The propagation constants' difference $\beta_i - \beta_j$ in tapered fiber also depends on the core diameter; accordingly, it changes along the taper length. If the pitch length is constant, the mode coupling coefficient is different along the taper length. Usually, only the fundamental mode was excited in the narrow part of the tapered fiber during experimental research. When the core diameter increases, the number of allowed propagation modes also increases, and, in the presence of mode coupling [in the fiber region where condition in Eq. (1) is fulfilled], the mode composition may change. Figure 10(a) shows the inverse difference in propagation constants (which determines the mode coupling coefficient [25]) for several low-order mode pairs as a function of position along the sT-DCF with 7.5 mm pitch.

The period of spatial modulation of the cladding diameter for the sT-DCF fiber with a 7.5 mm pitch in our case is the same everywhere and equals 1.88 mm ($\Lambda/4$, see Fig. 1). As follows from the simulation results, the resonant coupling period for the LP_{01} to LP_{11} pair is 1.2 mm, which is close to the real modulation period of 1.88 mm. The situation is aggravated by the fact that the sT-DCF has a constant length of about 1.5 m where the fiber diameter is almost constant, i.e., the fiber length, where the modulation period is most close to the resonant one, is very long. Removing this section significantly improves the beam quality (Fig. 9). Nevertheless, it should be noted that the experiment demonstrated a rather unexpected result: effective mode coupling in the core of the sT-DCF can arise even at the point where the spatial modulation period (1.88 mm) is far from the resonance condition (0.5 mm). Apparently, this is due to the fact that a real long fiber is always additionally bent, which complicates the frequency spectrum of spatial modulation.

Previously, we have observed a similar efficient mode coupling effect (Table 1 in [10]), where sT-DCF with a variable pitch length (2/13 mm) was used. The cladding diameter modulation period varied within the 0.5 to 3.25 mm range in [10], which closely corresponds to the results presented in this paper in Fig. 10(a). The output radiation of the sT-DCF was multimode when modulation periods of the cladding diameter were in the range of 0.5 to 1.5 mm (Table 1 in [10]). The

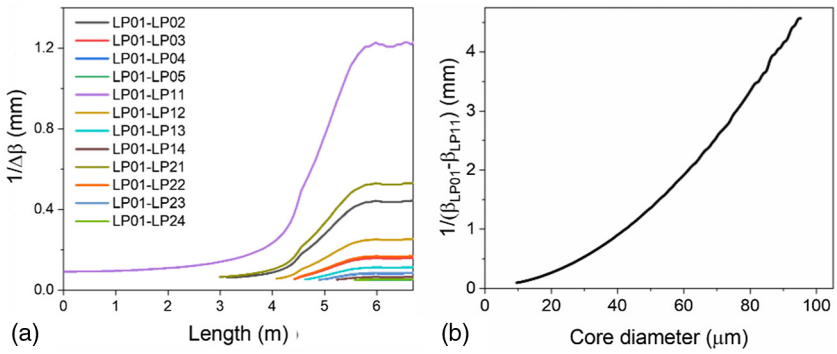

Fig. 10. (a) Inversed difference of propagation constants for LP01 and high-order modes versus position along the sT-DCF with 7.5 mm pitch. (b) Period of resonant modulation versus core diameter.

output light became single mode when the modulation period increased to $\Lambda > 1.5$ mm {Fig. 1(c), Table 1 in [10]}. Since our main goal is single-mode output, it is necessary to choose such parameters of the fiber core (diameter in the narrow end, Δn, and a pitch length) so that the following condition is fulfilled:

$$\Lambda > m/(\beta_{\mathrm{LP01}} - \beta_{\mathrm{LP11}}), \quad \textbf{(2)}$$

where β_{LP01} and β_{LP11} are propagation constants of transverse modes of the sT-DCF. In the general case, the condition in Eq. (2) should be valid along the whole length of the fiber. However, for sT-DCF with constant pitch length, it should be sufficient to require the condition to be met only in the wide part of the sT-DCF. The sT-DCF parameters (pitch length, Δn, and core diameter) should be chosen so that there is no point of efficient mode coupling along its length. In this sense, it is desirable to keep minimal the number of clad truncations m (one or two).

The large active core diameters (>50 μm and even more) are always desirable. Therefore, it is of interest to simulate the resonant coupling conditions for the LP_{01} and LP_{11} modes depending on the core diameter in the wide part. Figure 10(b) shows the dependence of the resonant coupling period versus core diameter.

As follows from the simulation results, for a 100 μm core diameter, a period of resonant longitudinal modulation of the cladding diameter (or other parameters) should be more than 5 mm. Thus, from the point of view of the mode content (avoiding the effective mode coupling conditions), the following conclusions can be made:

- Effective mode coupling can occur with periodic disturbance of outer cladding of sT-DCF due to a complex combination of periodical spinning disturbance, unpredictable diameter variations, and unavoidable fiber bending (spinning disturbance with a period of 1.88 mm caused coupling at the point where the resonance corresponds to 0.5 mm, Figs. 9 and 10(a).
- To avoid the appearance of the mode coupling, the number of cladding truncations should be minimized ($m = 1,\ 2,$ n but not 4) in order to increase the modulation period length of the cladding diameter.
- Since the period of the resonant mode coupling increases with the core diameter [Fig. 10(b)], it is also desirable to have a large pitch length in order to achieve a large MFD.

As follows from Fig. 10(b), the resonant period of longitudinal modulation is 5 mm for a 100 μm core. Taking into account that mode coupling begins even before the resonance for twice truncated cladding, the optimal pitch length for such a fiber should be 30 mm or more.

Polarization eigenstates of sT-DCF have been determined by the Jones method, and they are close to circular polarization (Table S1 in Supplement 1). Linear birefringence for all manufactured fibers is about 6.6×10^{-9} and determined by 75 cm diameter coiling. Circular intrinsic birefringence is determined by residual frozen-in twisting stresses, and it is about two times higher for a fiber with a 15 mm pitch (7.6×10^{-8}) compared with sT-DCF with 30 mm pitch length (3.4×10^{-8}). Since our goal is to create a fiber with the lowest possible intrinsic birefringence, in this sense, sT-DCF with a pitch of 30 mm seems to be preferable.

There are two ways for the pump radiation to vanish in active sT-DCF: light might be absorbed by an Yb-doped core, or it can leave the cladding through the side wall due to vignetting. The first effect is positive; the second is undesirable. In any case, when we measure the pump loss at the sT-DCF, we are dealing with a combination of both effects.

A smaller pitch length is achieved by faster preform rotation during the fiber drawing. The viscosity of molten quartz is finite and, at certain (sufficiently high) rotation speeds, internal residual frozen-in twisting mechanical stresses arise significantly, which lead to spatial modulation of the refractive index in the cross-section of an sT-DCF clad. Four waveguides are formed at the corners of the clad at the sT-DCF with a 7.5 mm pitch (Fig. 4). The unabsorbed pump intensity is concentrated at the very edge of the clad (in corners, see Fig. 4), which ultimately leads to pump leakage from the cladding. In the sT-DCF with a 15 mm pitch, a ring-shaped waveguide structure is also formed in the cladding (Fig. 4), where the unabsorbed pump is predominantly propagated without any absorption in the core, and this also reduces the efficiency of amplification. The ring-shaped waveguide associated with residual twisting stresses is no longer visible at the sT-DCF with 30 mm pitch (Fig. 4) compared with sT-DCFs with 7.5 and 15 mm pitch. Accordingly, the 30 mm pitch sT-DCF in the sense of frozen twisting stresses is quite similar to a nontwisted conventional T-DCF (Fig. 4), and it is better in terms of cladding pump absorption.

The total pump losses (Yb absorption plus vignetting) in a standard T-DCF and in a 30 mm pitch do not differ so much (1.7 and 2.0 dB/m, Table 1), while the slope efficiency differs significantly (57% and 74%, respectively). This means that twisting of the fiber offers significant improvement in the pump absorption of the active core [23]. As follows from the results shown in Fig. 7(b), the slope efficiency (i.e., the efficiency of a pump absorption by ytterbium) increases significantly with increasing pitch length, although the total pump losses (Yb absorption and vignetting) decrease. At some point, the slope efficiency will start to decrease to equal the slope efficiency of a regular T-DCF. Thus, pitch length should have an optimum to be determined in further research. Residual twisting stresses in the cladding, which are more significant at short pitches (7.5 and 15 mm), create additional waveguides in the cladding that do not intersect anyhow with the Yb-doped core, and this phenomenon ultimately leads to an increase in pump vignetting with shortening of a pitch length. Thus, fiber with a longer pitch (30 mm) is preferable from the point of view of better slope efficiency (74%), resulting in higher amplifier output power [Fig. 7(a)]. Since the ultimate goal is to create an efficient amplifier with sT-DCF, we can conclude that spun tapered fibers with a longer pitch (30 mm) are preferable in our case.

In this work, we have demonstrated the possibility of efficient frequency doubling (48% of conversion efficiency) of the light amplified in the MOPA system with sT-DCF (see Supplement 1). The stability of the green light output power was mainly determined by the temperature stability of the nonlinear crystal oven.

We can draw a conclusion based on our results:

- By rotating the preform during drawing, a fiber with low internal birefringence and small retardance can be produced

($\sim 10^{-8}$). This, in turn, makes SOP insensitive to heating caused by a quantum defect. According to our results, the output SOP in sT-DCF is practically independent of the pump power up to 100 W of the output power.

- The spinning of the preform with shaped cladding can cause mode coupling in the core, resulting in mode content degradation. To avoid it, the pitch length, core parameters, and cladding shape should be selected in accordance with the condition in Eq. (2).
- The spinning of shaped preform improves the clad pump absorption. However, a short pitch length (less than 30 mm) also causes excessive pump vignetting and eventually degradation of the gain properties (slope efficiency). Therefore, to avoid excessive pump vignetting, the pitch length should be 30 mm or longer.

4. CONCLUSION

In this work, we carried out a comprehensive comparative study of a novel type of Yb-doped spun tapered double-clad fibers with three different constant pitch lengths (7.5, 15, and 30 mm) and optimized geometry. Active spun tapered fiber with low near circular intrinsic birefringence $\sim 10^{-8}$ and constant pitch lengths were manufactured for the first time to our best knowledge.

We have demonstrated experimentally that the DOP and the SOP of the amplified light are weakly dependent on the pump power launched into the cladding revealing good polarization stability of the amplified light at a high output power level. Gain properties of an sT-DCF as a function of pitch length were investigated in detail. In particular, we discovered that, at certain pitch lengths, periodic modulation of the clad diameter caused by twisting of the shaped fiber leads to effective mode coupling, which, in turn, leads to mode content degradation. We have proposed conditions for choosing sT-DCF parameters in order to avoid effective mode coupling.

The influence of fiber twisting on the cladding pump absorption at sT-DCF was also studied. We found that, at certain pitch lengths (15 mm and shorter), waveguide structures appear in the sT-DCF cladding, channeling the pump radiation and preventing it from being efficiently absorbed by Yb ions located in the core. On the other hand, it has been experimentally confirmed that twisting a fiber with a certain pitch length definitely improves the clad mode mixing and improves the gain properties of the sT-DCF. Thus, we experimentally found that a 30 mm pitch is closest to optimal for our conditions.

Using an sT-DCF amplifier with 31 μm MFD ($M^2 < 1.2$) at 1064 nm, a picosecond MOPA system with 74% slope efficiency, 71 W output power, and 7 kW peak power was demonstrated. SOP was insensitive to the launched pump power. Output radiation (95 ps, 10/100 MHz) was frequency-doubled, and a green 532 nm laser with an output power of 17 W, peak power of 17 kW, and 80 pm linewidth was presented.

Funding. Academy of Finland (320165); Ministry of Science and Higher Education of the Russian Federation (0030-2019 0015).

Disclosures. V.U.: Ampliconyx Ltd. (E), J.R.: Ampliconyx Ltd. (E), T.N.: Ampliconyx Ltd. (E,I), R.G.: Ampliconyx Ltd. (I), Y.C. (P), V.F.: Ampliconyx Ltd. (E,P,I).

Data Availability. Data underlying the results presented in this paper are not publicly available at this time but may be obtained from the authors upon reasonable request.

Supplemental document. See Supplement 1 for supporting content.

REFERENCES

1. D. A. V. Kliner, J. P. Koplow, L. Goldberg, A. L. G. Carter, and J. A. Digweed, "Polarization-maintaining amplifier employing double-clad bow-tie fiber," Opt. Lett. **26**, 184–186 (2001).
2. O. Schmidt, J. Rothhardt, T. Eidam, F. Röser, J. Limpert, A. Tünnermann, K. Hansen, C. Jakobsen, and J. Broeng, "Single-polarization large-mode-area Yb-doped photonic crystal fiber," in *Conference on Lasers and ElectroOptics/Quantum Electronics and Laser Science Conference and Photonic Applications Systems Technologies* (Optical Society of America, 2008), paper CMB2.
3. A. Fedotov, T. Noronen, R. Gumenyuk, V. Ustimchik, Y. Chamorovskii, K. Golant, M. Odnoblyudov, J. Rissanen, T. Niemi, and V. Filippov, "Ultra-large core birefringent Yb-doped tapered double clad fiber for high power amplifiers," Opt. Express **26**, 6581–6592 (2018).
4. A. Ourmazd, M. P. Varnham, R. D. Birch, and D. N. Payne, "Thermal properties of highly birefringent optical fibers and preforms," Appl. Opt. **22**, 2374–2379 (1983).
5. S. C. Rashleigh and M. J. Marrone, "Temperature dependence of stress birefringence in an elliptically clad fiber," Opt. Lett. **8**, 127–129 (1983).
6. S. Rashleigh, "Origins and control of polarization effects in single-mode fibers," J. Lightwave Technol. **1**, 312–331 (1983).
7. I. Kaminow, "Polarization in optical fibers," IEEE J. Quantum Electron. **17**, 15–22 (1981).
8. D. C. Brown and H. J. Hoffman, "Thermal, stress, and thermo-optic effects in high average power double-clad silica fiber lasers," IEEE J. Quantum Electron. **37**, 207–217 (2001).
9. F. Wellmann, M. Steinke, F. Meylahn, N. Bode, B. Willke, L. Overmeyer, P. Weßels, J. Neumann, and D. Kracht, "Low-noise, single-frequency 200 W fiber amplifier," Proc. SPIE **11260**, 125–131 (2020).
10. J. Rissanen, A. Fedotov, T. Noronen, R. Gumenyuk, Yu. Chamorovskiy, A. Kolosovskii, V. Voloshin, I. Vorobev, M. Odnoblyudov, and V. Filippov, "Large-mode-area double clad ytterbium-doped tapered fiber with circular birefringence," Proc. SPIE **10897**, 342–394 (2019).
11. A. Fedotov, V. Ustimchik, Y. Chamorovskii, R. Gumenyuk, and V. Filippov, "Low-birefringence active tapered fibers for high-power applications," in *OSA Advanced Photonics Congress (AP) 2020 (IPR, NP, NOMA, Networks, PVLED, PSC, SPPCom, SOF)* (Optical Society of America, 2020), paper SoTu2H.7.
12. A. Fedotov, V. Ustimchik, J. Rissanen, A. Kolosovskii, V. Voloshin, I. Vorob'ev, R. Gumenyuk, Yu. Chamorovskiy, and V. Filippov, "Active tapered double-clad fiber with low birefringence," Opt. Express **29**, 16506–16519 (2021).
13. A. Fedotov, V. Ustimchik, J. Rissanen, T. Noronen, R. Gumenyuk, Yu. Chamorovskiy, A. Kolosovskii, V. Voloshin, I. Vorob'ev, and V. Filippov, "Large mode area double-clad ytterbium-doped tapered fiber with low birefringence," Proc. SPIE **11665**, 116651T (2021).
14. Yu. Chamorovskiy, N. Starostin, M. Ryabko, A. Sazonov, S. Morshnev, V. Gubin, I. Vorob'ev, and S. Nikitov, "Miniature microstructured fiber coil with high magneto-optical sensitivity," Opt. Commun. **282**, 4618–4621 (2009).
15. F. Just, H.-R. Müller, S. Unger, J. Kirchhof, V. Reichel, and H. Bartelt, "Ytterbium-doping related stresses in preforms for high-power fiber lasers," J. Lightwave Technol. **27**, 2111–2116 (2009).
16. G. W. Scherer, "Stress-induced index profile distortion in optical waveguides," Appl. Opt. **19**, 2000–2006 (1980).
17. O. E. Shushpanov, A. N. Tuzov, I. V. Alexsandrov, S. P. Vikulov, M. E. Zhabotinskii, V. V. Romanovtzev, and S. J. Feld, "An automated system for measurement of mechanical stresses in optical fiber preforms with polarization-optical method," Radiotechnika **43**, 67–72 (1988).
18. M. R. Hutsel, R. Ingle, and T. K. Gaylord, "Accurate cross-sectional stress profiling of optical fibers," Appl. Opt. **48**, 4985–4995 (2009).

19. Z. Lou, B. Yang, K. Han, X. Wang, H. Zhang, X. Xi, and Z. Liu, "Real-time in-situ distributed fiber core temperature measurement in hundred-watt fiber laser oscillator pumped by 915/976 nm LD sources," Sci. Rep. **10**, 9006 (2020).
20. F. Just, R. Spittel, J. Bierlich, S. Grimm, M. Jäger, and H. Bartelt, "The influence of the fiber drawing process on intrinsic stress and the resulting birefringence optimization of PM fibers," Opt. Mater. **42**, 345–350 (2015).
21. A. J. Barlow, J. J. Ramskov-Hansen, and D. N. Payne, "Birefringence and polarization mode-dispersion in spun single-mode fibers," Appl. Opt. **20**, 2962–2968 (1981).
22. D. N. Payne, A. J. Barlow, and J. J. Ramskov-Hansen, "Development of low- and high-birefringence optical fibers," IEEE Trans. Microw. Theory Tech. **30**, 323–334 (1982).
23. P. Koška, P. Peterka, J. Aubrecht, O. Podrazký, F. Todorov, M. Becker, Y. Baravets, P. Honzátko, and I. Kašík, "Enhanced pump absorption efficiency in coiled and twisted double-clad thulium-doped fibers," Opt. Express **24**, 102–107 (2016).
24. D. Kouznetsov and J. Moloney, "Efficiency of pump absorption in double-clad fiber amplifiers. II. Broken circular symmetry," J. Opt. Soc. Am. B **19**, 1259–1263 (2002).
25. D. Marcuse, *Light Transmission Optics* (Van Nostrand Reinold, 1972).